

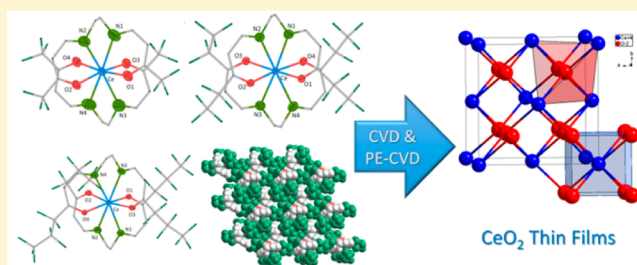
Fluorinated Cerium(IV) Enaminolates: Alternative Precursors for Chemical Vapor Deposition of CeO₂ Thin Films

J. Schläfer, D. Graf, G. Fornalczyk, A. Mettenböcker, and S. Mathur*

Institute of Inorganic Chemistry, University of Cologne Greinstraße 6, D-50939 Cologne, Germany

Supporting Information

ABSTRACT: High-yield synthesis of four new fluorinated enaminones LH₂ (R_fC(O)C₂H₂NH)₂C₂H₄ (R_f = CF₃ (2a), C₂F₅ (2b), C₃F₇ (2c)) and (F₃CC(O)C₂H₂NH)₂C₃H₆ (2a') as dianionic ligands is described. The ligands were characterized in solution (via nuclear magnetic resonance (NMR)) as well as in the solid state (via X-ray diffraction (XRD)). The ligating ability of the enaminones was verified by reacting them with [Ce₂(OⁱPr)₈(HOⁱPr)₂], which resulted in monomeric cerium(IV) complexes [CeL₂] (3a–c, 3a') based on tetradentate chelation of the ligands. Cerium enaminolates were comprehensively analyzed by NMR spectroscopy, mass spectrometry, and single-crystal XRD studies to verify their monomeric nature. High stability under ambient conditions and high volatility makes them a potential precursor for the gas-phase synthesis of CeO₂. Complexes 3a and 3b were applied as precursors in thermal and plasma-enhanced chemical vapor deposition to obtain crystalline ceria films with different surface morphologies. The purity and surface states of the films were analyzed by X-ray photoelectron spectroscopy, which revealed a high amount of Ce³⁺ on the subsurface of CeO₂ films.



INTRODUCTION

Thin films of ceria, which is a cubic fluorite-type oxide ($Fm\bar{3}m$), have attracted considerable attention, because of their optoelectronic and insulating properties (band gap of 3.2 eV) as well as their unique redox chemistry, accompanied by excellent oxygen storage capacity.^{1–4} These superior characteristics highlight the potential of CeO₂-based materials in numerous technological applications, e.g., luminescent layers,⁵ high refractive materials,⁶ catalysis,⁷ gas sensors⁸ and fuel cells.⁹ For the preparation of ceria thin films, several physical and chemical synthetic methods have been applied, for example, gas-phase methods such as pulsed laser deposition (PLD),^{10,11} metal-organic chemical vapor deposition (MOCVD),^{12,13} atomic layer deposition (ALD),^{14–17} or solution-based methods.^{18,19} In this context, chemical vapor deposition (CVD) is a versatile coating technique, which offers decisive advantages including conformal step coverage, large deposition area, and better controllability over material properties and composition. Use of plasma-enhanced deposition (PECVD) allows film preparation under nonequilibrium conditions, usually at low temperatures, which results in film characteristics that are not obtainable by other deposition techniques. So far, the preparation of ceria thin films via PECVD has been reported only once, based on application of [Ce(dpm)₄] (dpm = 2,2,6,6-tetramethyl-3,5-heptadionate) as a precursor.²⁰

Design of volatile precursors for gas-phase depositions of rare-earth oxides is a tedious challenge, because of the large ionic radius of lanthanide cations and their high atomic weight, which often results in the formation of polymeric compounds and/or nonvolatile complexes.^{21,22} Metal alkoxides are

frequently used as single-source precursors for metal oxides, despite their high reactivity against moisture, largely because of their high structural diversity and clean decomposition behavior at low temperatures.^{23–26} Nevertheless, volatile cerium(IV) alkoxides are limited to few examples, such as [Ce₂(OMe₂Pr)₈].²⁷ Moreover, most of the known derivatives exhibit only moderate stability at room temperature or under light irradiation.^{28–32} By deploying chelating ligands such as bidentate β-diketonates,^{12,14,20,33,34} fluorinated heteroarylalkenolates,³⁵ or donor-functionalized alkoxide ligands³⁶ stable, mononuclear complexes could be obtained, some of them showing reasonable volatility, although at elevated temperatures (see Scheme 1).

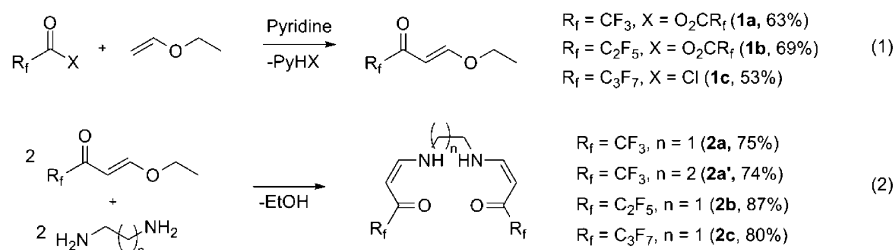
Scheme 1. Qualitative Evaluation of Stability, Volatility, and Decomposition Properties of Different Precursor Classes for Gas-Phase Deposition of CeO₂^a

	Cerium(IV) Alkoxides		Cerium(IV) β-Diketonates		
Stability	-	+	+	++	-
Volatility	+	++	-	+	++
Decomposition	++	--	++	+	+

^aLegend: (++) excellent, (+) good, (-) poor, (--) not sufficient; X = O, N; R_f = perfluoroalkyl group.

Received: February 20, 2016

Scheme 2. Two-Step Synthesis of Enaminones 2a–c and 2a'



Herein, we present high-yield synthesis of new tetradentate ligands that could be easily synthesized starting from nonexpensive, commercially available chemicals. This good affordability and high volatility of resulting monomeric cerium complexes offer access to an attractive precursor class that matches or even outperforms the established cerium(IV) β -diketonate complexes for economic reasons, as well as because of improved physicochemical properties. This claim was demonstrated by CVD experiments with **3a** and **3b** that produce homogeneous CeO_2 films.

RESULTS AND DISCUSSION

Synthesis and Characterization of Enaminones. The enaminones were synthesized in a two-step procedure in high yields, according to Scheme 2. In a first step, β -ethoxyvinyl perfluoroalkyl ketones were prepared following a standard procedure by acylation of ethoxyethylene with acid anhydride or acid chlorides containing the polyfluoroalkyl groups $R_f = CF_3$ (**1a**), C_2F_5 (**1b**), and C_3F_7 (**1c**), respectively (eq 1 in Scheme 2).^{37,38} The liquid compounds could be purified by distillation under reduced pressure and were analyzed by NMR spectroscopy and elemental analysis. Finally, **1a–c** were reacted with ethylenediamine or trimethylenediamine in a nucleophilic reaction, resulting in the formation of the enaminones LH_2 ($R_fC(O)C_2H_2N_{H_2}C_2H_4$ ($R_f = CF_3$ (**2a**), C_2F_5 (**2b**), C_3F_7 (**2c**)) and $(F_3CC(O)C_2H_2NH)_2C_3H_6$ (**2a'**) (eq 2 in Scheme 2). The compounds were isolated from the reaction medium in high analytical purity as colorless crystals via recrystallization from dichloromethane or chloroform in high yields ($\geq 74\%$).

The 1H NMR spectra of the ligands in $CDCl_3$ exhibited similar patterns consisting of four (**2a–c**) or five (**2a'**) characteristic resonances, respectively, which could be assigned to NH protons (10.3 ppm), allylic protons (4.5 ppm (d), 7.0 ppm (dd)), and the protons of diaminoalkyl backbone (3.5 ppm, 2.0 ppm). The attachment of an acidic proton to the nitrogen of the enamine function was confirmed by the $^3J_{HH}$ coupling to the allylic proton (H2). The protons of the double bond (H2, H3) showed a $^3J_{HH}$ coupling constant of 7 Hz, indicating that the existence of *Z*-isomers in solution offers additional stabilization, because of the formation of intramolecular $N-H\cdots O$ hydrogen bonds. The formation of *E*-isomers could be induced by altering the polarity of the solvent, which was investigated for the derivative **2a** in an exemplary NMR study (Table 1). Polar solvents weaken the bonding energy of the hydrogen bridge by donating electron density to the heteroatoms and thereby facilitate the formation of *E*-isomers manifested in an additional resonance for H3 shifted to lower field with a coupling constant of 13 Hz. In more-polar solvents, the coexistence of both isomers was observed while the *E*:*Z* ratio increased with increasing polarity, reaching the maximum ratio of 63:37 in $DMSO-d_6$ solution. The ligands were comprehensively characterized by ^{13}C and ^{19}F NMR one-

Table 1. Ratio of *E*- and *Z*-Isomers of **2a** in Different Solvents Determined by 1H NMR Integration of Signals Corresponding to Allylic Protons^a

solvent	donor number	Content (%)	
		<i>E</i> -isomer	<i>Z</i> -isomer
chloroform- <i>d</i>	n/a	0	100
nitromethane- <i>d</i> ₃	2.7	11	89
acetonitrile- <i>d</i> ₃	14.1	18	82
THF- <i>d</i> ₈	20.0	20	80
$DMSO-d_6$	29.8	63	37

^aDonor numbers were taken from the literature (values are given for protonated solvents).³⁹

dimensional (1D) and two-dimensional (2D) experiments; the full data set and assignments are given in the Experimental Section.

Crystals of compounds **2a** and **2b** were analyzed in the solid state by single-crystal diffraction. (Molecular structures of **2a** and **2b** are shown in Figure 1.) The ligands crystallize in the triclinic space group $P\bar{1}$ ($Z = 1$) and the monoclinic space group $I2_1/c$ ($Z = 4$), respectively (see Table 2). In agreement with the NMR findings, both ligands exclusively form the *Z*-isomer but distinguish themselves by adopting different rotamer forms produced by rotation about the ethylene diamine backbone. The formation of the energetically unfavorable gauche conformer observed for **2b** is most likely caused by crystal packing effects. The description of the molecular structure by an enaminon tautomeric form is supported by the C2–N (1.305 Å) and C4–O (1.223 and 1.235 Å) bond lengths, which are in good agreement with those typically found for C=O and C=N double bonds.

Cerium(IV) Enaminolates. Cerium complexes **3a–c** and **3a'** were prepared in a straightforward one-step synthesis by reacting $[Ce_2(O'Pr)_8(HO'Pr)_2]$ with 4 equiv of ligand HL_2 in THF at room temperature. Reaction occurred immediately indicated by color change from yellow to intense purple. The products were purified by vacuum sublimation and were obtained as deep red powders in nearly quantitative yields ($\geq 95\%$). The sublimation temperature was found to decrease with increasing fluorine contents (from 140 °C to 110 °C, 10^{-2} mbar), which could be explained by a more pronounced repulsion among negatively polarized fluorine groups of adjacent molecules that eventually weakens intermolecular attractive forces. Introduction of a diaminopropane backbone, on the other hand, did not have any beneficial effect on the thermal properties of the resulting cerium complex. In contrast, the sublimation point of **3a'** (155 °C, 10^{-2} mbar) is higher than those of **3a–c**. Mass spectra (EI, 20 eV) recorded for complexes confirmed their good volatility and stability in the gas phase showing the molecular ion peak $[M]^+$ as a main fragment.

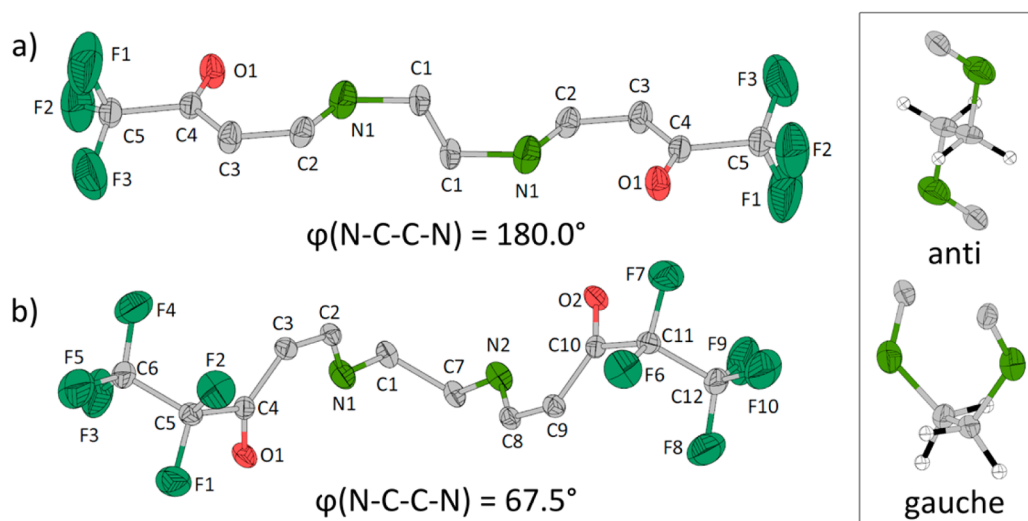


Figure 1. Molecular structures of (a) **2a** and (b) **2b**. Thermal ellipsoids are shown at 30% probability level, and the hydrogen atoms have been omitted for the sake of clarity. The rotational conformation about the ethylene diamine backbone is depicted in the inset on the right side (φ is the dihedral angle).

Table 2. Crystal and Structure Refinement Data for **2a**, **2b**, and **3a–c**

parameter	2a	2b	3a	3b	3c
formula	$\text{C}_{10}\text{H}_{10}\text{N}_2\text{O}_2\text{F}_6$	$\text{C}_{12}\text{H}_{16}\text{N}_4\text{O}_4\text{F}_{10}$	$\text{CeC}_{20}\text{H}_{16}\text{N}_4\text{O}_4\text{F}_{12}$	$\text{CeC}_{24}\text{H}_{16}\text{N}_4\text{O}_4\text{F}_{20}$	$\text{CeC}_{28}\text{H}_{16}\text{N}_4\text{O}_4\text{F}_{28}$
M_r (g mol ⁻¹)	304.2	404.2	744.34	944.53	1144.57
cryst syst	triclinic	monoclinic	monoclinic	monoclinic	triclinic
space group	$P\bar{1}$	$I2_1/c$	Pc	$P2_1/c$	$P\bar{1}$
T (K)	293(2)	170(2)	293(2)	293(2)	293(2)
a (Å)	5.7104(7)	13.329(4)	11.343(5)	15.814(5)	10.050(5)
b (Å)	7.3062(8)	6.542(5)	13.833(5)	10.652(5)	13.882(5)
c (Å)	8.209(1)	17.975(6)	9.061(5)	19.012(5)	14.422(5)
α (°)	109.75(2)	90.00	90.00	90.00	102.131(5)
β (°)	101.39(2)	94.41(4)	110.025(5)	91.656(5)	107.985(5)
γ (°)	97.17(1)	90.00	90.00	90.00	90.183(5)
V (Å ³)	309.10(7)	1562.7(14)	1335.8(2)	3201(2)	1866.0(13)
Z	1	4	2	4	2
μ (Mo $K\alpha$) (mm ⁻¹)	0.173	0.195	1.822	1.577	1.402
No. of unique rflns, R_{int}	1370, 0.0370	1661, 0.0718	5716, 0.1898	6782, 0.0583	7876, 0.0743
goodness of fit	0.992	1.066	0.993	1.046	1.088
final R indices [$I > 2\sigma(I)$]: R_1 , wR_2	0.0419, 0.1056	0.0349, 0.0878	0.0708, 0.0775	0.0361, 0.0460	0.0317, 0.0426
R indices (all data): R_1 , wR_2	0.0611, 0.1120	0.0440, 0.0946	0.1750, 0.1819	0.0913, 0.1014	0.0757, 0.0861
residual electron density	0.256, -0.154	0.219, -0.225	2.460, -1.205	0.808, -1.410	0.697, -0.946

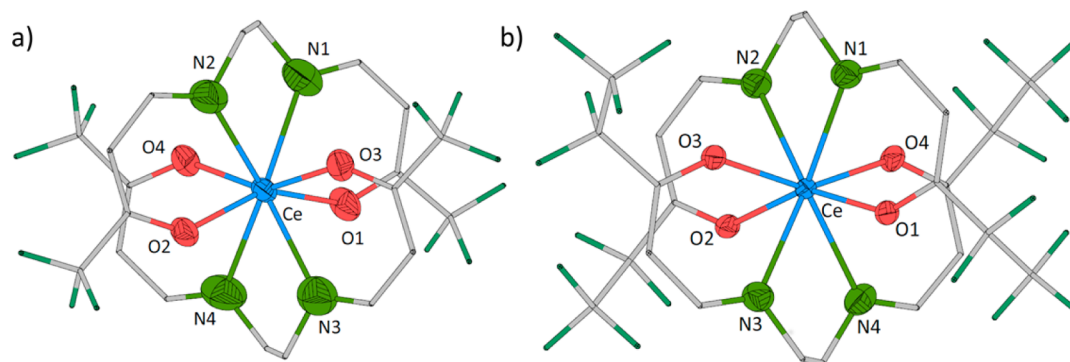


Figure 2. Molecular structures of (a) **3a** and (b) **3b**. Thermal ellipsoids for Ce, N, and O atoms are shown at 30% probability level, and the H atoms have been omitted for the sake of clarity. Selected bond lengths [Å]: (a) Ce–O1 2.232(6), Ce–O2 2.256(6), Ce–O3 2.248(7), Ce–O4 2.210(8), Ce–N1 2.535(7), Ce–N2 2.543(7), Ce–N3 2.549(9), Ce–N4 2.552(7); (b) Ce–O1 2.246(3), Ce–O2 2.241(3), Ce–O3 2.236(2), Ce–O4 2.235(3), Ce–N1 2.537(3), Ce–N2 2.537(3), Ce–N3 2.537(3), Ce–N4 2.532(3).

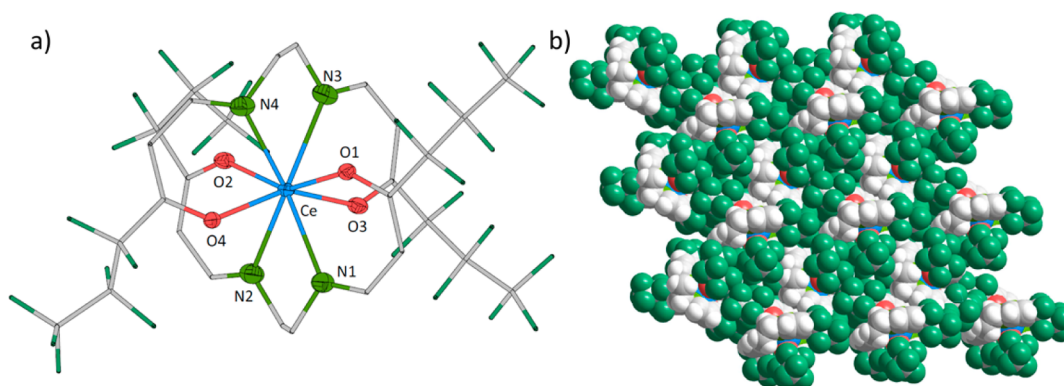


Figure 3. (a) Molecular structure of **3c**. Thermal ellipsoids for Ce, N, O atoms are shown at 30% probability level, and the hydrogen atoms have been omitted for clarity. Selected bond lengths [Å]: Ce–O1 2.258(2), Ce–O2 2.209(2), Ce–O3 2.231(2), Ce–O4 2.272(2), Ce–N1 2.537(3), Ce–N2 2.557(3), Ce–N3 2.586(3), Ce–N4 2.519(3). (b) Space-filling model of the crystal structure of **3c**. View along *a*-axis.

In contrast to the free ligands, all complexes exhibited a good solubility in organic solvents and were studied in solution by multinuclear NMR spectroscopy. A pronounced chemical shift of signals in the ^1H , ^{13}C , and ^{19}F NMR spectra as well as the absence of NH proton resonance corroborate the coordination of enaminolate ligands to the metal center. Furthermore, the rigid ligation geometry prevents free rotation about the alkyl diamine backbone allowing vicinal proton–proton coupling of aliphatic protons, which results in the detection of a singlet for **3a–c** or a triplet and a quintet for **3a'**, respectively.

Compounds **3a–c** were analyzed in the solid state using single-crystal diffraction experiments. The complexes showed distorted trigonal dodecahedral coordination with perpendicular arrangement of two ligands coordinating the Ce center (see Figures 2 and 3). The gauche conformation of the ligand allowed for an almost-planar alignment of binding N and O sites which coordinate the metal center under the formation of stable 6- and 5-membered chelate rings. The average Ce–O bond lengths of 2.240 Å are between those typically found for terminal alkoxo groups (1.960–2.146 Å)^{30–32} and cerium(IV) β -diketonates (2.318–2.393 Å)^{12,14,20,33,34} and match those observed for fluorinated heteroarylalkenolates (2.188–2.216 Å)³⁵ suggesting an enaminolate resonance structure. The mean Ce–N atomic distances of 2.543 Å are in good agreement with those reported for Schiff-Base complexes of tetravalent cerium.⁴⁰ The extension of the perfluoroalkyl end groups has no significant influence on the molecular structure or bond lengths and angles of the metal-organic complexes but it does alter the packing of molecules in the crystal. In the crystal structure, fluorine and nonfluorine domains of the complexes pack together, becoming more pronounced as the fluorine content increases (Figure 3). This phenomenon is believed to be triggered by intermolecular noncovalent interactions, e.g., hydrogen bonding and electrostatic interactions whereas the influence of fluorophilic interactions on the molecular packing is still the subject of controversial discussions.^{41,42} The increased volatility of the fluorinated metal complexes is possibly due to the low polarizability of the F atom, as well as the high electronegativity, giving rise to relatively weak C–F...F–C interactions (1–20 kcal mol^{−1}) and significant electrostatic repulsion, which result in low intermolecular attraction.

Chemical Vapor Deposition of CeO₂. The low sublimation temperature of the metal-organic compounds and their high stability under ambient conditions makes them attractive candidates for cerium oxide deposition processes;

these properties make them highly desirable, because of their technological potential (catalyst, UV absorbers, sensing). Compounds **3a** and **3b** were chosen as precursors for preliminary experiments, unifying a high volatility with good affordability of the starting materials. The thermogravimetric profiles of both complexes at a heating rate of 10 °C/min showed the establishment of a sharp mass loss at 200 °C, because of sublimation, which passes into a decomposition step at ~300 °C (see Figures S12 and S13 in the Supporting Information). The high vapor pressure of **3b** results in a massive weight loss of 88%, exceeding the theoretical value of 82% by assuming a clean decomposition to ceria. In contrast, the mass loss of 64% for **3a** is higher than the theoretical one of 77%, indicating the incorporation of impurities in the decomposition product.

Compounds **3a** and **3b** were tested in both thermal and plasma-enhanced CVD (PECVD). In thermal CVD, a precursor temperature of 135 °C (**3a**) was applied, whereas the pressure was adjusted to 5×10^{-3} mbar at a deposition temperature of 700 °C. In PECVD experiments, the precursor temperature was set at 150 °C (3.5×10^{-2} mbar) (**3a** and **3b**), deploying 10 sccm of argon as carrier gas. PECVD resulted in the formation of amorphous films whereas thermal CVD gave rise to crystalline deposits. The samples were annealed in air at 500 °C for 2 h in order to initiate the crystallization process and to remove any carbon impurities. Subject to the nature of energy supply, SEM images of the samples exhibited differences in film morphology (Figure 4). While thermally treated films exhibited a granular structure with an average grain size of 50 nm, plasma-deposited films showed a surface structure with low surface roughness and conformal coverage of the substrate. In both processes, poor adhesion of the ceria layer to Si(100) substrate was observed. The formation of crystalline ceria phase

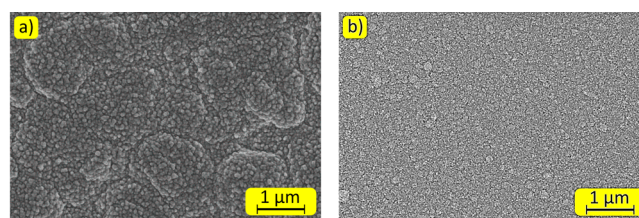


Figure 4. SEM micrographs illustrating the different surface morphology of ceria films grown by (a) thermal CVD and (b) plasma-enhanced CVD on polycrystalline alumina substrates.

has been corroborated by powder X-ray diffraction (XRD) and the observed reflexes were consistent with the cubic fluorite-type structure (JCPDS No. 34-0394); see Figure 5). The higher

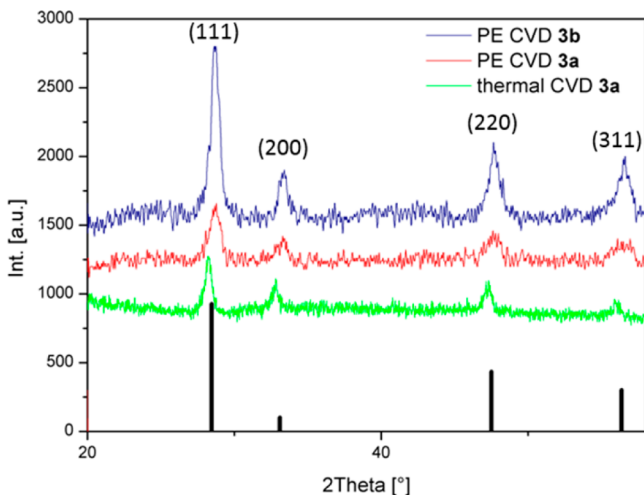


Figure 5. X-ray diffraction (XRD) pattern of ceria films obtained by thermal CVD (3a) and plasma-enhanced CVD (3a and 3b).

peak intensity observed for the depositions carried out with 3b can be explained by higher film thickness due to an increased vapor pressure of the precursor. Calculations using the Scherrer formula revealed similar small crystallite sizes for all samples. Films obtained by thermal CVD exhibited a mean crystallite size of 11.3 nm, whereas the plasma-deposited films showed an average of 13.8 nm (3a) and 10.8 nm (3b).

Films were analyzed by XPS measurements in order to exclude the formation of amorphous byproducts such as CeF_3 . The survey scans of the plasma deposits showed exclusively peaks for carbon, oxygen, and cerium, indicating a clean ligand strip-off without incorporation of fluorine or nitrogen impurities in the films. High-resolution XPS spectrum of Ce 3d levels was recorded and was fitted with a sum of Gaussian–Lorentzian functions with variable contributions (Figure 6). It is composed of two series of multiplets (denoted as “u” and “v”, corresponding to $3d_{5/2}$ and $3d_{3/2}$ states caused by spin–orbit

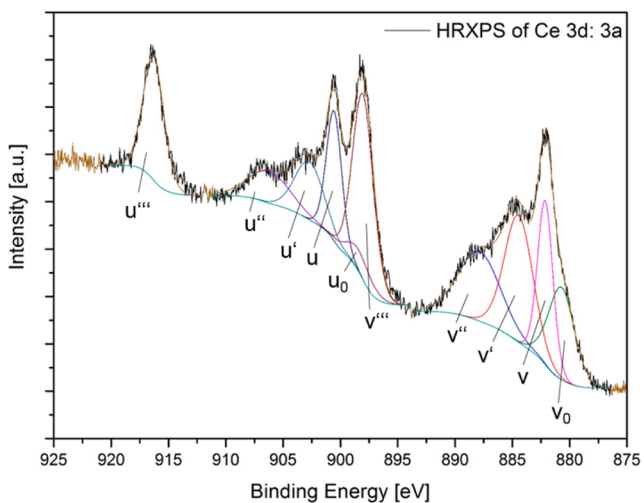


Figure 6. High-resolution XPS spectrum of Ce 3d levels in the sample synthesized by PECVD using precursor 3a.

splitting. The individual peaks can be correlated to Ce(IV) (denoted as v, v'', and v''' in Figure 6) and Ce(III) (denoted as u, u', and u'' in Figure 6). The same fitting was applied to the u lines in Figure 6, revealing the presence of a high amount of Ce^{3+} ions on the surface of the ceria films (up to 38%), which indicates a high defect concentration.^{43,44} Survey scan of the deposit obtained by thermal CVD showed a higher amount of carbon that could be drastically reduced by argon sputtering of the sample, suggesting the predominance of surface carbon species. The contamination either originates from the graphite susceptor used to inductively heat the substrates or by an incomplete decomposition of the organic ligand sphere, which could be circumvented by the use of a reactive gas such as oxygen in order to promote the decomposition of the precursor. The survey scans of the sputtered samples show no fluorine content, excluding the formation of a CeF_3 phase.

It could be shown that the precursors already evaporate at considerably low temperatures in the reactor and decompose to CeO_2 without the formation of undesired contaminations. The use of additional co-reactants, such as oxygen, is not necessary in the case of thermal CVD, although it evidently promotes the precursor decomposition. Direct influence of the precursor chemistry on the film morphology is difficult to evaluate with the current set of data, which are meant to provide the proof-of-principle. Film properties are strongly dependent on the chosen method, reaction conditions, and reactor design, which restricts comparative analyses of CeO_2 films obtained from different precursors. CVD of ceria generally requires co-reactants, such as O_2 , and carrier gases or solvents. Only the report by Hoffmann and co-workers describes the deposition of ceria using the single-source precursor $[\text{Ce}_2(\text{OCMe}_2\text{Pr})_8]$, without any co-reactant.²⁷ The nanosized, grainlike film morphology and high crystallinity of those films were similar to those reported in this paper. In good agreement with our results, Barecca et al. obtained ceria films with a small grain size (~ 5 nm) by deploying the β -diketonate precursor $[\text{Ce}(\text{dpm})_4]$ in PECVD.²⁰ The $\text{Ce}^{3+}/\text{Ce}^{4+}$ ratio was heavily dependent on the supply of argon and O_2 gases into the reaction chamber, for instance, a high oxygen partial pressure was found to result in a lower amount of Ce^{3+} . Our experiments have demonstrated that the new cerium enaminate complexes show high vapor pressures and can be easily transported to the decomposition zone at considerably low evaporation temperatures to obtain CeO_2 films using different reactor designs.

CONCLUSION

The development of stable, easy-to-handle rare-earth metal–organic precursors, which exhibit high vapor pressure and good decomposition behavior is still a challenging task. Judicious choice of chelating ligands can check the oligomerization and enforce the formation of monomers exhibiting high molecular stability. Nevertheless, a lower degree of nuclearity is not the only criterion to enhance volatility, and the role of intermolecular interactions is also crucial. Minimization of intermolecular attraction that is often achieved by increasing the electrostatic repulsion, e.g., by introducing negatively polarized perfluoroalkyl groups in the ligand periphery, which can also impart higher stability under ambient conditions due to a hydrophobic molecular exterior. On the other hand, the use of fluorinated compounds in CVD processes is also reported to result in a contamination of deposits by metal fluorides such as CeF_3 , which diminish their potential application as precursors.

In this paper, we reported an easy and reliable synthesis of a new dianionic, tetradentate enaminone ligands starting from inexpensive and readily available chemicals. Chelating enaminones (**2a–c**, **2a'**) were able to accommodate the high ionic radius of Ce⁴⁺ cation allowing the isolation of highly volatile, air-stable compounds in high yields. Contrary to other fluorinated cerium complexes, depositions using the novel cerium complexes **3a** and **3b** resulted exclusively in the formation of cubic CeO₂, both in thermal CVD as well as PECVD, showing no evidence of fluorine incorporation. These findings suggest that precursors based on the new enaminone ligands allow compromising the high volatility of fluorinated complexes with the deposition of fluorine-free films via different gas-phase techniques. Moreover, the syntheses of ligands can be easily modified in order to change the type and number of the donor sites as well as the organic backbone of the ligand to extend the coordination chemistry to a broad range of metal cations.

EXPERIMENTAL SECTION

Precursor Synthesis. General Remarks. If not mentioned specifically, all reagents and solvents were used without further purification. The syntheses of cerium complexes were carried out under dry nitrogen gas atmosphere; solvents were dried over sodium and distilled prior to use. Pentafluoropropionic anhydride and heptafluorobutyl chloride were prepared by refluxing the corresponding acid with P₄O₁₀ or PCl₅, respectively. Compounds **1a–c** were synthesized following a literature procedure; the synthetic protocols and analytical data can be found in the [Supporting Information](#). [Ce₂(OⁱPr)₈(HOⁱPr)₂] was synthesized according to literature methods.⁴⁵ NMR spectra were recorded on a Bruker Model Avance II 300 spectrometer. ¹H (300.1 MHz), ¹³C (75.7 MHz), and ¹⁹F (282.5 MHz) chemical shifts are reported in parts per million (ppm), relative to external tetramethylsilane or CCl₃F, and are referenced internally to the proton impurity or ¹³C signal of the solvent, respectively. Mass spectra were recorded on a Finnigan MAT 95 (EI, 20 eV) in *m/z* (intensity, in %). Elemental analyses were carried out on a HEKATECH CHNS Euro EA 3000. DTA measurements were performed on a TGA/DSC1 (Mettler–Toledo GmbH, Gießen, Germany) apparatus. Data collection for X-ray structure elucidation was performed on a STOE IPDS II diffractometer using graphite-monochromated Mo K α radiation (0.71071 Å). The programs used in this work are STOE's X-Area and the WINGX suite of programs, including SIR-92 and SHELXL-97 for structure solution and refinement. H atoms were calculated geometrically and a riding model was applied during the refinement process. Structure of complex **3a** was solved in acentric space group *Pc*, which gave a Flack parameter of 0.80(4) indicating the presence of racemic twinning; therefore, the structure was refined as an inversion twin.

Synthesis of *N,N'*-bis(4,4,4-trifluorobut-1-en-3-one)-ethylenediamine (2a**).** 25.0 g (150 mmol) of **1a** was slowly added to a solution of 4.50 g (75 mmol) of ethylenediamine in 50 mL of dichloromethane. The reaction mixture was stirred for 2 h at room temperature and the white precipitate was isolated by filtration. 17.03 g (75%) of the product were obtained as colorless crystals from a concentrated dichloromethane solution. Melting point (Mp) = 165 °C. ¹H NMR (CDCl₃, 25 °C): δ 3.55 (m, 4H, H1), 5.42 (d, ³J_{HH} = 7.25 Hz, 2H, H3), 7.02 (dd, ³J_{HH} = 7.25 Hz, 12.26 Hz, 2H, H2), 10.20 (s, 2H, NH). ¹³C NMR (CDCl₃, 25 °C): δ 50.2 (C1), 88.0 (C3), 117.0 (C5), 157.3 (C2), 179.0 (C4). ¹⁹F NMR (CDCl₃, 25 °C): δ -77.0 (s, ¹J_{CF} = 288 Hz, ²J_{CF} = 32 Hz). EI-MS (20 eV, 110 °C): *m/z* (intensity) 304 [M]⁺ (56%), 165 (100%), 151 (96%), 113 (11%), 84 (20%). Anal. Calcd C₁₀H₁₀N₂O₂F₆: C 39.48, H 3.31, N 9.21. Found: C 39.94, H 3.62, N 9.39.

Synthesis of *N,N'*-bis(4,4,5,5,5-pentafluoropent-1-en-3-one)-ethylenediamine (2b**).** The synthetic procedure was similar to that described for **2a**, starting from 11.49 g (53 mmol) of **1b**. 9.34 g (87%) of the product were obtained as colorless crystal from a concentrated

chloroform solution. Mp = 155 °C. ¹H NMR (CDCl₃, 25 °C): δ 3.57 (m, 4H, H1), 5.50 (d, ³J_{HH} = 7.20 Hz, 2H, H3), 7.02 (dd, ³J_{HH} = 7.22 Hz, 13.05 Hz, 2H, H2), 10.28 (s, 2H, NH). ¹³C NMR (CDCl₃, 25 °C): δ 50.1 (C1), 89.5 (C3), 107.6 (C5), 118.3 (C6), 157.6 (C2), 180.3 (C4). ¹⁹F NMR (CDCl₃, 25 °C): δ -82.6 (s, ¹J_{CF} = 286 Hz, ²J_{CF} = 37 Hz, 3F, F6), -123.5 (s, ¹J_{CF} = 263 Hz, ²J_{CF} = 35 Hz, 2F, F5). EI-MS (20 eV, 105 °C): *m/z* (intensity) 404 [M]⁺ (60%), 257 [M-C₂F₃(CO)]⁺ (18%), 215 (98%), 202 (100%), 190 (10%), 84 (20%). Anal. Calcd C₁₂H₁₀N₂O₂F₁₀: C 35.66, H 2.59, N 6.93. Found: C 35.53, H 2.65, N 6.34.

Synthesis of *N,N'*-bis(4,4,5,5,6,6,6-heptafluorohex-1-en-3-one)-ethylenediamine (2c**).** The synthetic procedure was similar to that described for **2a**, starting from 5.70 g (21 mmol) of **1c**. 4.24 g (80%) of the product were obtained as pale yellow crystals from a concentrated dichloromethane solution. Mp = 130 °C. ¹H NMR (CDCl₃, 25 °C): δ 3.57 (m, 4H, H1), 5.47 (d, ³J_{HH} = 7.18 Hz, 2H, H3), 7.01 (dd, ³J_{HH} = 7.11 Hz, 13.07 Hz, 2H, H2), 10.27 (s, 2H, NH). ¹³C NMR (CDCl₃, 25 °C): δ 50.1 (C1), 90.1 (C3), 113.9 (C5), 123.5 (C6), 132.7 (C7), 157.6 (C2), 179.8 (C4). ¹⁹F NMR (CDCl₃, 25 °C): δ -80.7 (t, ¹J_{CF} = 288 Hz, ³J_{FF} = 9 Hz, 3F, F7), -121.4 (q, ¹J_{CF} = 266 Hz, ³J_{FF} = 9 Hz, 2F, F5), -127.1 (s, ¹J_{CF} = 266 Hz, 2F, F6). EI-MS (20 eV, 96 °C): *m/z* (intensity) 504 [M]⁺ (60%), 335 [M-C₃F₇]⁺ (12%), 305 [M-C₃F₇(CO)]⁺ (22%), 265 (100%), 252 (98%), 240 (12%), 84 (24%). Anal. Calcd C₁₄H₁₀N₂O₂F₁₄: C 33.25, H 2.19, N 5.47.

Synthesis of *N,N'*-bis(4,4,4-trifluorobut-1-en-3-one)-propylenediamine (2a'**).** The synthetic procedure was similar to that described for **2a**, starting from 2.58 g (43 mmol) of **1a**. 4.05 g (74%) of the product were obtained as pale yellow crystals from a concentrated dichloromethane solution. ¹H NMR (CDCl₃, 25 °C): δ 2.00 (qui, 2H, H1'), 3.47 (q, 4H, H1), 5.44 (d, ³J_{HH} = 7.12 Hz, 4H, H3), 7.13 (dd, ³J_{HH} = 7.12 Hz, 13.40 Hz, 4H, H2), 10.24 (s, 2H, NH). ¹⁹F NMR (CDCl₃, 25 °C): δ -77.0. Anal. Calcd C₁₄H₁₀N₂O₂F₁₄: C 41.52, H 3.80, N 8.80. Found: C 41.33, H 3.56, N 9.28.

Synthesis of **3a.** To a solution of 0.63 g (0.72 mmol) [Ce₂(OⁱPr)₈(HOⁱPr)₂], a portion of **2a** (0.88 g, 2.88 mmol) was added and stirred at room temperature for 30 min. The reaction mixture was evaporated to dryness and the crude product was purified by vacuum sublimation at 140 °C (10⁻² mbar). 1.01 g (95%) of **3a** were obtained as a deep red solid. Mp = 151 °C. ¹H NMR (CDCl₃, 25 °C): δ 3.51 (s, 8H, H1), 5.13 (d, ³J_{HH} = 5.18 Hz, 4H, H3), 7.08 (d, ³J_{HH} = 5.18 Hz, 4H, H2). ¹³C NMR (CDCl₃, 25 °C): δ 64.9 (C1), 97.1 (C3), 135.8 (C5), 157.9 (C2), 174.4 (C4). ¹⁹F NMR (CDCl₃, 25 °C): δ -73.9. EI-MS (20 eV, 105 °C): *m/z* (intensity) 744 [M]⁺ (100%), 593 [CeN₃O₃C₁₅H₁₂F₉]⁺ (22%), 552 [CeN₄O₃C₁₅H₁₄F₆]⁺ (62%), 442 [M-L]⁺ (62%). Anal. Calcd CeO₄N₄C₂₀H₁₆F₁₂: C 32.27, H 2.17, N 7.53. Found: C 32.20, H 2.76, N 6.80.

Synthesis of **3b.** The synthetic procedure was similar to that described for **3a**, starting from 0.56 g (0.64 mmol) [Ce₂(OⁱPr)₈(HOⁱPr)₂] and 1.06 g (2.56 mmol) **2b**. The crude product was purified by vacuum sublimation at 135 °C (10⁻² mbar). 0.91 g (96%) of **3b** were obtained as a deep red solid. Mp = 119 °C. ¹H NMR (CDCl₃, 25 °C): δ 3.69 (s, 8H, H1), 5.25 (d, ³J_{HH} = 5.28 Hz, 4H, H3), 7.23 (d, ³J_{HH} = 5.28 Hz, 4H, H2). ¹⁹F NMR (CDCl₃, 25 °C): δ -72.9 (s, 12F, F6), -121.9 (s, 8F, F5). EI-MS (20 eV, 99 °C): *m/z* (intensity) 944 [M]⁺ (100%), 742 [CeN₃O₃C₁₈H₁₂F₁₅]⁺ (18%), 701 [CeN₄O₃C₁₈H₁₄F₁₂]⁺ (19%), 542 [M-L]⁺ (21%). Anal. Calcd CeO₄N₄C₂₄H₁₆F₂₀: C 30.52, H 1.71, N 5.93. Found: C 30.50, H 1.69, N 5.45.

Synthesis of **3c.** The synthetic procedure was similar to that described for **3a**, starting from 0.19 g (0.22 mmol) [Ce₂(OⁱPr)₈(HOⁱPr)₂] and 0.44 g (0.87 mmol) **2c**. The crude product was purified by vacuum sublimation at 110 °C (10⁻² mbar). 0.24 g (95%) of **3c** were obtained as a deep red solid. Mp = 98 °C. ¹H NMR (CDCl₃, 25 °C): δ 4.18 (s, 8H, H1), 5.36 (d, ³J_{HH} = 4.89 Hz, 4H, H3), 8.05 (d, ³J_{HH} = 4.86 Hz, 4H, H2). ¹³C NMR (CDCl₃, 25 °C): δ 62.8 (C1), 99.5 (C3), 108.6 (C6), 111.70 (C5), 118.0 (C7), 159.0 (C2), 160.1 (C4). ¹⁹F NMR (CDCl₃, 25 °C): δ -80.89 (t, 12F, ³J_{FF} = 8.98 Hz, F7), -119.75 (q, 8F, ³J_{FF} = 8.97 Hz, F5), -127.07 (s, 8F, F6). EI-MS (20 eV, 86 °C): *m/z* (intensity) 1142 [M]⁺ (100%), 893

[CeN₃O₃C₂₁H₁₃F₂₁]⁺ (15%), 852 [CeN₄O₃C₂₁H₁₄F₁₈]⁺ (17%), 642 [M-L]⁺ (20%). Anal. Calcd CeO₄N₄C₂₈H₁₆F₂₈: C 29.38, H 1.41, N 4.90. Found: C 29.71, H 1.49, N 4.26.

Synthesis of 3a'. The synthetic procedure was similar to that described for 3a, starting from 0.45 g (0.51 mmol) [Ce₂(OⁱPr)₈(HOⁱPr)₂] and 0.65 g (2.05 mmol) 2a'. The crude product was purified by vacuum sublimation at 155 °C (10⁻² mbar). 0.24 g (95%) of 3a' were obtained as a deep red solid. Mp = 181 °C. ¹H NMR (CDCl₃, 25 °C): δ 2.12 (d, ³J_{HH} = 6.78 Hz, 4H, H1'), 4.34 (t, ³J_{HH} = 6.60 Hz, 8H, H1), 5.45 (d, ³J_{HH} = 5.17 Hz, 4H, H3), 8.09 (d, ³J_{HH} = 5.19 Hz, 4H, H2). ¹³C NMR (CDCl₃, 25 °C): δ 31.5 (C1'), 56.1 (C1), 98.2 (C3), 120.2 (C6), 159.3 (C5), 161.3 (C2). ¹⁹F NMR (CDCl₃, 25 °C): δ -73.8. EI-MS (20 eV, 135 °C): m/z (intensity) 772 [M]⁺ (100%), 456 [M-L]⁺ (8%). Anal. Calcd CeO₄N₄C₂₂H₂₀F₁₂: C 34.20, H 2.61, N 7.25. Found: C 34.25, H 3.06, N 6.97.

CVD Experiments. Thermal CVD. Experiments were performed in a horizontal CVD reactor in which a high-frequency field was used to inductively heat the silicon substrates by placing them on a graphite susceptor. The molecular precursors were introduced in the reactor through a glass flange by applying a dynamic vacuum (5 × 10⁻³ mbar) and heating the precursor reservoir to the desired temperature.

PE CVD Experiments. Thin ceria films were deposited by using radio frequency (RF, 13.56 MHz) plasma CVD with an RF power of 75 W at room temperature. The external precursor vessel and the precursor feeding lines were heated at 150 °C by heating tapes. 10 sccm of argon and 10 sccm of oxygen were used as reactive gas and 10 sccm of argon as carrier gas. The as-deposited amorphous layers were calcined under air at 600 °C for 3 h.

Material Characterization. Room-temperature powder X-ray diffraction (XRD) was obtained on a STOE-STADI MP diffractometer operating in the reflection mode using Cu Kα (λ = 1.5406 Å) radiation. The microstructures of the samples were examined using field-emission scanning electron microscopy (FEI Nova NanoSEM 430 and Zeiss Neon 40). X-ray photoemission spectroscopy (XPS) was performed on ESCA M-Probe (Al Kα) with an energy resolution of 0.8 eV.

■ ASSOCIATED CONTENT

● Supporting Information

The Supporting Information is available free of charge on the ACS Publications website at DOI: [10.1021/acs.inorgchem.6b00348](https://doi.org/10.1021/acs.inorgchem.6b00348).

Synthesis methodologies, NMR, thermogravimetry–differential thermal analysis (TGA-DTA), and XPS spectra (PDF)

Crystallographic data for C₁₀H₁₀F₆N₂O₂ (CIF)

■ AUTHOR INFORMATION

Corresponding Author

*E-mail: sanjay.mathur@uni-koeln.de.

Notes

The authors declare no competing financial interest.

■ ACKNOWLEDGMENTS

The authors gratefully acknowledge the financial support provided by the University of Cologne and the European Commission for partial funding under the WIROX contract No. PIRSE-GA-2011-295216 (Marie Curie Action). We are grateful to Dr. I. Pantenburg for crystal structure determination and Mr. A. Sasinska for XPS evaluation.

■ REFERENCES

- (1) Sun, C.; Li, H.; Chen, L. *Energy Environ. Sci.* **2012**, *5*, 8475–8505.
- (2) Trovarelli, A. *Catal. Rev.: Sci. Eng.* **1996**, *38*, 439–520.

(3) Nachimuthu, P.; Shih, W.-C.; Liu, R.-S.; Jang, L.-Y.; Chen, J.-M. *J. Solid State Chem.* **2000**, *149*, 408–413.

(4) Deshpande, S.; Patil, S.; Kuchibhatla, S. V.; Seal, S. *Appl. Phys. Lett.* **2005**, *87*, 133113.

(5) Fujihara, S.; Oikawa, M. *J. Appl. Phys.* **2004**, *95*, 8002–8006.

(6) Mogensen, M.; Sammes, N. M.; Tompsett, G. A. *Solid State Ionics* **2000**, *129*, 63–94.

(7) Trovarelli, A.; de Leitenburg, C.; Boaro, M.; Dolcetti, G. *Catal. Today* **1999**, *50*, 353–367.

(8) Brosha, E. L.; Mukundan, R.; Brown, D. R.; Garzon, F. H.; Visser, J. *Solid State Ionics* **2002**, *148*, 61–69.

(9) Park, S.; Vohs, J. M.; Gorte, R. J. *Nature* **2000**, *404*, 265–267.

(10) Skofronick, G. L.; Carim, A. H.; Foltyn, S. R.; Muenchausen, R. E. *J. Mater. Res.* **1993**, *8*, 2785–2798.

(11) Rodrigo, K.; Wang, H.; Heiroth, S.; Pryds, N.; Kuhn, L. T.; Esposito, V.; Linderth, S.; Schou, J.; Lippert, T. *Appl. Surf. Sci.* **2011**, *257*, 5341–5346.

(12) Becht, M.; Morishita, T. *Chem. Vap. Deposition* **1996**, *2*, 191–197.

(13) Pan, M.; Meng, G.; Xin, H.; Chen, C.; Peng, D.; Lin, Y. *Thin Solid Films* **1998**, *324*, 89–93.

(14) Paivasaari, J.; Putkonen, M.; Niinisto, L. *J. Mater. Chem.* **2002**, *12*, 1828–1832.

(15) Maeng, W. J.; Oh, I.-K.; Kim, W.-H.; Kim, M.-K.; Lee, C.-W.; Lansalot-Matras, C.; Thompson, D.; Chu, S.; Kim, H. *Appl. Surf. Sci.* **2014**, *321*, 214–218.

(16) Lee, S.; Oh, S.; Goo, D.; Youm, D. *Thin Solid Films* **1995**, *258*, 299–304.

(17) Guo, S.; Arwin, H.; Jacobsen, S. N.; Järrendahl, K.; Helmersson, U. *J. Appl. Phys.* **1995**, *77*, 5369–5376.

(18) Kamada, K.; Higashikawa, K.; Inada, M.; Enomoto, N.; Hojo, J. *J. Phys. Chem. C* **2007**, *111*, 14508–14513.

(19) Kuzmina, N. P.; Ibragimov, S. A.; Makarevich, A. M.; Martynova, I. A.; Kharchenko, A. V.; Korolev, V. V.; Kardashov, S. V. *Chem. Mater.* **2010**, *22*, 5803–5813.

(20) Barreca, D.; Gasparotto, A.; Tondello, E.; Sada, C.; Polizzi, S.; Benedetti, A. *Chem. Vap. Deposition* **2003**, *9*, 199–206.

(21) Aspinall, H. C.; Bickley, J. F.; Gaskell, J. M.; Jones, A. C.; Labat, G.; Chalker, P. R.; Williams, P. A. *Inorg. Chem.* **2007**, *46*, 5852–5860.

(22) Boyle, T. J.; Ottley, L. A. M. *Chem. Rev.* **2008**, *108*, 1896–1917.

(23) Hemmer, E.; Huch, V.; Adlung, M.; Wickleder, C.; Mathur, S. *Eur. J. Inorg. Chem.* **2011**, *2011*, 2148–2157.

(24) Zamani, R.; Fiz, R.; Pan, J.; Fischer, T.; Mathur, S.; Morante, J. R.; Arbiol, J. *CrystEngComm* **2013**, *15*, 4532–4539.

(25) Müller, R.; Hernandez-Ramirez, F.; Shen, H.; Du, H.; Mader, W.; Mathur, S. *Chem. Mater.* **2012**, *24*, 4028–4035.

(26) Pan, J.; Shen, H.; Werner, U.; Prades, J. D.; Hernandez-Ramirez, F.; Soldera, F.; Mücklich, F.; Mathur, S. *J. Phys. Chem. C* **2011**, *115*, 15191–15197.

(27) Suh, S.; Guan, J.; Miinea, L. A.; Lehn, J.-S. M.; Hoffman, D. M. *Chem. Mater.* **2004**, *16*, 1667–1673.

(28) Sirio, C.; Hubert-Pfalzgraf, L. G.; Bois, C. *Polyhedron* **1997**, *16*, 1129–1136.

(29) Yunlu, K.; Gradeff, P. S.; Edelstein, N.; Kot, W.; Shalimoff, G.; Streib, W. E.; Vaartstra, B. A.; Caulton, K. G. *Inorg. Chem.* **1991**, *30*, 2317–2321.

(30) Schläfer, J.; Stucky, S.; Tyrre, W.; Mathur, S. *Inorg. Chem.* **2013**, *52*, 4002–4010.

(31) Schläfer, J.; Tyrre, W.; Mathur, S. *Inorg. Chem.* **2014**, *53*, 2751–2753.

(32) Evans, W. J.; Deming, T. J.; Olofson, J. M.; Ziller, J. W. *Inorg. Chem.* **1989**, *28*, 4027–4034.

(33) Becht, M.; Gerfin, T.; Dahmen, K.-H. *Chem. Mater.* **1993**, *5*, 137–144.

(34) McAleese, J.; Plakatouras, J. C.; Steele, B. C. H. *Thin Solid Films* **1996**, *280*, 152–159.

(35) Lehnen, T.; Schläfer, J.; Mathur, S. *Z. Anorg. Allg. Chem.* **2014**, *640*, 819–825.

- (36) Aspinall, H. C.; Bacsa, J.; Jones, A. C.; Wrench, J. S.; Black, K.; Chalker, P. R.; King, P. J.; Marshall, P.; Werner, M.; Davies, H. O.; Odedra, R. *Inorg. Chem.* **2011**, *50*, 11644–11652.
- (37) Hojo, M.; Masuda, R.; Kokuryo, Y.; Shioda, H.; Matsuo, S. *Chem. Lett.* **1976**, *5*, 499–502.
- (38) Gorbunova, M. G.; Gerus, I. I.; Kukhar, V. P. *Synthesis* **2000**, *2000*, 738–742.
- (39) Huheey, J.; Keiter, E.; Keiter, R. *Anorganische Chemie, Prinzipien von Struktur und Reaktivität*, 3rd Edition; de Gruyter: Berlin, 2003.
- (40) Gao, B.; Zhang, Q.; Yan, P.; Hou, G.; Li, G. *CrystEngComm* **2013**, *15*, 4167–4175.
- (41) Chopra, D.; Row, T. N. G. *CrystEngComm* **2011**, *13*, 2175–2186.
- (42) Baker, R. J.; Colavita, P. E.; Murphy, D. M.; Platts, J. A.; Wallis, J. D. *J. Phys. Chem. A* **2012**, *116*, 1435–1444.
- (43) Pfau, A.; Schierbaum, K. *Surf. Sci.* **1994**, *321*, 71–80.
- (44) Bêche, E.; Charvin, P.; Perarnau, D.; Abanades, S.; Flamant, G. *Surf. Interface Anal.* **2008**, *40*, 264–267.
- (45) Toledano, P.; Ribot, F.; Sanchez, C. *Acta Crystallogr., Sect. C: Cryst. Struct. Commun.* **1990**, *46*, 1419–1422.